Study of the influence of micro- and nano-cellulose on the growth and carbonation kinetics of portlandite crystals

Paulina Guzmán García Lascurain[1*], *Carlos* Rodríguez-Navarro[2], *Irene* De Giuli[1], *Lucia* Toniolo[1], and *Sara* Goidanich[1]

[1]Department of Chemistry, Materials and Chemical Engineering 'Giulio Natta', Politecnico di Milano, Italy
[2]Departamento Mineralogia y Petrologia, Universidad de Granada, Fuentenueva s/n, 18002 Granada, Spain

Abstract. Restoration of historical buildings contributes to the preservation of history and identity of the cities, but also, in the current climate crisis, an alternative solution to reduce the environmental impact of the construction sector, which is one of the main global contributors to green-house gas emissions and waste production. It can be also claimed that the most sustainable building is the one that has already been built. An important aspect to consider for the restoration of built heritage is the use of compatible materials, such as lime-based mortars, that should be preferred over cement. However, their slow setting and hardening (via carbonation), and, in some cases, poor durability prevent their full acceptance and widespread use. One course of action is to improve the quality of the binder via an innovative approach: inclusion of natural organic additives during the slaking process of CaO. This is expected to have a higher impact than their inclusion in the mortar's mix design. In the present work the analysis of the growth of $Ca(OH)_2$ crystals following their crystallization in the presence of micro- and nano-cellulose is studied, together with the morphological changes that these additives induce on portlandite crystals. Moreover, the study of the carbonation kinetics of the modified portlandite crystals gives insights on the effect that these additives have on the quality of the binder. The promising results highlight the potential of micro- and nano-cellulose as sustainable additives for lime-based binders. Furthermore, these additives can be obtained from industrial wastes, promoting a circular economy.

1 Introduction

In the context of built heritage preservation, lime-based mortars should be preferred to cement, for non-structural interventions, given their high compatibility with the original masonry [1,2] and their lower environmental impact [3,4]. It is well known that the

* Corresponding author: paulina.guzman@polimi.it

These proceedings are published with the support of EuLA.

restoration of built heritage is crucial to preserve the historical identity of cities, but today restoration is also necessary to reduce the environmental impact of the construction industry. The building sector is responsible for around 37% of the global energy consumption and 27% of the global operational CO_2 emissions [5]; this means that to reach carbon neutrality in 2050, the emissions would need to decrease 98% from the 2020 reported levels [5]. It is imminent to take actions to decarbonize the construction industry, for example by limiting building new constructions and prolonging the lifetime of buildings through restoration. In Europe alone, more than 40% of the buildings are older than 50 years [6]. Therefore, their maintenance, restauration and repair are of great importance to prevent their decay, while promoting a culture of circular economy [7–9].

Aerial lime binders are obtained from limestone ($CaCO_3$) that is calcined at c.a. 950°C to obtain CaO, also known as quicklime. This white, reactive powder is then hydrated, resulting in slaked or hydrated lime ($Ca(OH)_2$, mineral portlandite). If water is added in excess to the CaO, the result will be a dispersion of $Ca(OH)_2$ particles known as lime putty. They are used for aerial lime-based mortars. After mixing with aggregates, the excess of water will first evaporate from the mortar causing a plastic shrinkage, then the binder will harden via carbonation, forming again $CaCO_3$ [10].

Carbonation is a slow process, influenced by many factors such as: temperature, relative humidity, porosity of the mortar, and quality of the employed binder [11,12]. This last factor is determined by the textural and structural properties of the portlandite crystals, which in turn may impact their reactivity [12]. In general, it has been reported that full carbonation, and thus complete hardening of the mortar, may take many years to be completed [13]. This is not suitable for today's construction and restoration requirements. The long waiting times needed for carbonation have provoked the replacement of lime-based mortars with gypsum or cement. These mortars are incompatible with the original masonry and will result in its damage [14,15]. Thus, it is necessary to improve the performance of lime-based mortars and the quality of the lime binders to promote their widespread use, particularly in the field of built heritage.

The implementation of additives is one of the most fruitful ways to improve the performance of lime-based mortars. Additives are materials incorporated, in reduced quantities, into mortar mixtures to enhance their working properties and long-term performance [10,16]. However, the introduction of additives may be expensive and challenging to scale-up to an industrial level. Furthermore, these materials improve the properties of the mortar but do not necessarily increase the quality of the binder *per se*. Since ancient times, high quality binders have been obtained through the maturation of the lime-putty [17,18]. Aged lime putty is characterized by a higher plasticity, workability, water retention, and faster carbonation rate [18]. These improvements are a consequence of the shape transformation of the prismatic $Ca(OH)_2$ crystals during aging. It has been reported that with time, the basal {00.1} faces of portlandite are preferentially formed while the prismatic {10.0} and {11.0} faces tend to disappear [18]. This leads to the formation of corrosion features along the (10.0) and (11.0) planes, observed on aged lime-putty [17,18]. The result is the transformation from large prismatic crystals to small plate-like ones. This increases the surface area of the portlandite crystals, and thus increases reactivity, promoting faster carbonation [19]. However, the effects of aging on lime putty are observed after years, making this process unprofitable and time-consuming [17,18]. It would thus be desirable to achieve these improved textural features of portlandite particles in a faster and more efficient way. One way to do so could be using additives (crystallization inhibitors and/or habit modifiers).

Recently, a novel approach for the use of additives has been explored [20–22]: their introduction during the hydration process of CaO rather than into the mortar mixture. This approach aims to directly modify the properties of the forming $Ca(OH)_2$ crystals for overall

improvement of the quality of slaked lime, by mimicking some of the features obtained during lime-putty aging. In their work, Kang et al. [21], demonstrated that the addition of salt and sugar to the slaking water led to contrasting results. On the one hand, slaking in the presence of salt generates a brief dormant period in the quicklime reaction with water. The result is a slight reduction on the $Ca(OH)_2$ particle size. On the other hand, the addition of sugar to the slaking water generates a considerable delay in the hydration of CaO, leading to smaller and less crystalline $Ca(OH)_2$ particles. Sugar does not inhibit the hydration reaction but hinders the growth of the portlandite crystals after their nucleation [21]. A similar effect has been observed with the addition of nopal juice extract and citrus pectin to the slaking water. These two additives acted as nucleation inhibitors producing nanometric crystals [20]. The explanation of their effect is based on the non-classical nucleation theory, which states that the process of mineral crystallization develops trough intermediate metastable steps, until reaching the final thermodynamically stable phase [23]. There are different pathways that crystallization can follow [24], one of particular interest is the two-step nucleation commonly observed in biomineralization systems as well as in biomimetic processes, following crystallization in aqueous solution [23]. During this process, stable prenucleation clusters (PNCs) will be formed and, over increasing saturation values, they will agglomerate. These grouped PNCs will then form a dense liquid. As the saturation of the solution continues to increase, a nucleation event will take place, from which the formation of an amorphous phase will take place followed by its transformation into a crystalline phase. Within the non-classical nucleation theory, additives can play different roles depending on their effect in the mineral precipitation. According to the classification proposed by Gebauer et al. [25,26], additives can be separated in at least nine types, one of which are nucleation inhibitors; these can act via stabilization or destabilization of PNCs [27]. Stabilization of the PNCs occurs when the additive's molecules are adsorbed during the pre-nucleation stage preventing the aggregation of PNCs. As a result, this delays phase separation to form the dense liquid. On the other hand, the destabilization of PNCs leads to their constant dissociation therefore hindering the formation of a new phase [20]. For the case of nopal juice and pectin used as additives included during the hydration of CaO, the authors proposed that the nucleation-inhibition effect occurs via the destabilization of PNCs in the case of nopal juice extract, and trough the stabilization of the PNCs when pectin was used [20]. Moreover, these additives act as habit modifier of the newly formed $Ca(OH)_2$ crystals. The adsorption of the additives on the forming (00.1) surfaces of portlandite, hinders aggregation and growth along the z direction. The result is a larger population of plate-like particles, such as those observed in aged lime putty [20].

Evidence shows that carbohydrates play a relevant part on the crystallization of calcium minerals like $Ca(OH)_2$ and $CaCO_3$ [20,21,27,28]: However, to the knowledge of the authors, these effects have not been thoroughly studied for the case of micro- and nano-cellulose. Cellulose is the most abundant natural biopolymer. It is a polysaccharide made of long chains of D-glucose units linked by a glycosidic bond; nano- and micro-cellulose differ only on the length of the linked units and thus on their crystallinity. Recently the application of micro- and nano-cellulose materials has proven to be a sustainable, low cost and non-toxic alternative to synthetic ingredients for many applications. Nonetheless, the use of micro- and nano-cellulose as additive to lime-based mortars has revealed contrasting results. Particularly in terms of the mechanical properties of the mortars, it is not yet clear the effect that these additives may have [29–31]. Therefore, it is difficult to determine a strong correlation between the mechanical properties and the added fibrils. On the other hand, the presence of nano-cellulose has proven to promote a biomimetic mineralization of $CaCO_3$ [32]. The authors found that spatial organization of the nano-cellulose fibres plays a fundamental role in determining the shape of calcite produced [32]. During the growth of calcium carbonate

crystals, the nano-cellulose acts as a scaffold for the deposition of Ca^{2+} ions thus controlling the growth of $CaCO_3$ [30,32–34].

In the present work the use of micro- and nano-cellulose is proposed as a sustainable additive for the hydration process of quicklime. Ultimately the aim is to improve the quality of the aerial lime. It is hypothesized that the cellulose fibrils will produce modifications to portlandite crystals morphology during their nucleation and growth process. The aim is to understand the interaction between micro- and nano-cellulose with $Ca(OH)_2$ during the different stages of formation of this mineral, and comprehend the consequences that their addition has on the carbonation process of portlandite.

2 Materials and Methods

2.1 Raw materials

To perform the $Ca(OH)_2$ synthesis, a 100mM solution of NaOH (Scharlau) and a 250 mM solution of $CaCl_2$ (Scharlau) were used. These solutions were prepared daily. Microfibrillated cellulose, Celova®, was provided by Weidmann (Switzerland). This material is characterized by a particle length between 8 and 10 µm. The material is provided in a high-water content dispersion, therefore, before use, it was oven dried for 36 h at 50°C. Nano-cellulose was synthetized via acid hydrolysis according to the methodology reported in the literature [35]. The precursor was 100% hydrophilic cotton. The hydrolysis process had a yield of 80%, resulting in a dispersion of nano-cellulose particles with an average size of 280 nm, measured by dynamic light scattering using a Zetasizer Nano instrument (Malvern Panalytical). The nano-cellulose was oven dried in the same conditions as the micro-cellulose.

2.2 Homogeneous synthesis of $Ca(OH)_2$

The effect of the additives on the formation of $Ca(OH)_2$ was evaluated using a computer-controlled titration system. All experiments were done in a Titrando 905 titrator manufactured by Methrom (Switzerland) following the methodology reported in [20]. A solution of NaOH (100 mM) was used as analyte, the different concentrations of micro- and nano-cellulose (10, 100, 1000, and 5000 ppm) were included into the analyte. Control samples without any cellulose were performed as well. To ensure the proper dispersion of the fibres, the NaOH solution with cellulose was sonicated for 15 min prior to starting the experiment. The titrant used was a solution of $CaCl_2$ (250 mM), added at a constant rate of 4 µL/s for four hours in a N_2 atmosphere. The reaction was monitored using a Ca^{2+} ion selective electrode (Combined Calcium ISE, Methrom), a pH glass electrode (Unitrode, Methrom) with a Pt1000 sensor for temperature monitoring, a conductivity probe (five-ring conductivity measuring cell, Methrom), and a transmittance probe at 610 nm (Optrode, Methrom). Once per day a calibration for the Ca^{2+} electrode was performed. For this a solution of NaCl (100 mM) was used as analyte and the reaction was performed using the same protocol previously described. All experiments were performed in triplicate to ensure reproducibility.

The obtained products were filtered and oven dried for 10 minutes at 60°C. Once dried they were stored in Eppendorf tubes filled with N_2 to prevent carbonation. Powder X-ray diffraction (XRD) on all the samples was performed using a Panalytical X'Pert Pro diffractometer equipped with Ni filter, working at 40 kV and 40 mA, Cu Kα radiation (λ = 1.5405 Å), in a 2θ range of 20-40°. XRD patterns were analysed using HighScore Software (Malvern Panalytical). Morphological analysis using scanning electron microscope was done

with a Phenom XL G2 Desktop SEM (ThermoFisher™ Scientific) at 15 kV acceleration voltage and pressure of 10 Pa.

2.3 Carbonation process

To follow the process of carbonation of $Ca(OH)_2$ over time, another set of samples was prepared following the same homogeneous reaction previously described. The reaction was done in a 100 mL solution of NaOH (100 mM) containing micro- or nano-cellulose (10 ppm, or 100 ppm) in a N_2 atmosphere. A $CaCl_2$ solution (250 mM, 60 mL) was added to the NaOH and left to react under constant stirring (500 rpm) and N_2 atmosphere for 90 minutes. A control sample without additives was also made in the same manner. All the resulting precipitates were filtered, oven dried (60°C for 10 minutes) and stored in an open Eppendorf tube to promote the natural carbonation process at room temperature and relative humidity of 60%.

The carbonation process was followed using macro-FTIR with a Nicolet™ iS20 spectrometer module by ThermoFisher™ Scientific, equipped with a DTGS detector and a Smart itX™ diamond accessory for Attenuated Total Reflection (ATR) in the spectral range 4000 - 400 cm^{-1}, collecting 64 scans for each measurement with a 4 cm^{-1} spectral resolution (diameter of the crystal 2 mm). Spectra were collected at 0, 1, 5, 12, 15, and 20 days. Additionally, XRD analyses of samples carbonated for 20 days were performed.

3 Results and Discussion

3.1 Influence of cellulose on portlandite nucleation

It is known from literature that polysaccharides act as nucleation inhibitors in the formation of calcium hydroxide [27]. Although the effect of micro- and nano-cellulose on the formation of $Ca(OH)_2$ has not been tested yet, the evidence observed for other polysaccharides allows to hypothesize that cellulose would behave similarly. Therefore, the effect of these additives was tested following the time evolution of $Ca(OH)_2$ formation in the presence of increasing concentrations of the additives. The results from the time evolution of the free Ca^{2+} ions in the titration reactions can be observed in Fig. **1**. In all cases it was possible to observe that the slope of the Ca^{2+} evolution is less steep than the experimentally dosed Ca^{2+} (dashed line). This indicates that part of the available calcium ions in solution were consumed by the formation of PNCs [27] even in the control runs. These species are thermodynamically stable with no phase boundary [36] and in this case they form and coexist with the ions in solution. The latter contributes to the validation that the mineral precipitation of $Ca(OH)_2$ follows a non-classical pathway.

In Fig. **1** it is possible to observe that cellulose (micro and nano) acts as a nucleation inhibitor. This is evidenced by the delay of the nucleation event (marked by a drop in the free Ca^{2+} signal). In addition, it is possible to see that the inhibition effect is dependent on the concentration of micro- and nano-cellulose, except for nano cellulose at low concentration (10 ppm), where nucleation is promoted. As explained in the introduction, nucleation inhibition can occur by stabilization or destabilization of PNCs. An additive that causes nucleation inhibition via PNCs stabilization, would provoke a reduction in the slope of the free Ca^{2+} evolution over time with respect to the control. The results show that for most of the tested cases micro- and nano-cellulose stabilize the PNCs, thus resulting in a delay of the nucleation event. Only micro-cellulose at 100 ppm and nano-cellulose at 1000 ppm have a slope comparable to the control. For the other cases, the inhibition occurs via stabilization, indicating that a larger quantity of pre-nucleation clusters is present in the solution without

agglomerating. For nano-cellulose, a concentration dependence on the delay effect, specially at high concentrations (100 ppm or more), was expected, considering previous similar experiments with nopal juice and other additives [20,22,27]. Instead, when micro-cellulose was used, at high concentrations (1000 and 5000 ppm), the nucleation is apparently inhibited for the whole duration of the experiment. Moreover, there were no differences between 1000 ppm and 5000 ppm of added micro-cellulose. It is also worth noticing that the slope of the curve is significantly shallower for these concentrations of micro-cellulose, indicating a strong stabilization of PNCs. Conversely, at low amounts (10 and 100 ppm) of micro-cellulose, the nucleation occurs as expected from the literature regarding nopal juice, pectin, and other organic additives [20,22,27].

The delay in the nucleation can have important implications on the morphology of the newly formed $Ca(OH)_2$ crystals. A change in crystal habit has been reported in the presence of nucleation inhibition additives, where portlandite crystals tend to have a plate-like configuration rather than a prismatic one [20]. This is interesting since it resembles the effect that aging has on lime putty [17], without having to wait for a long period of time.

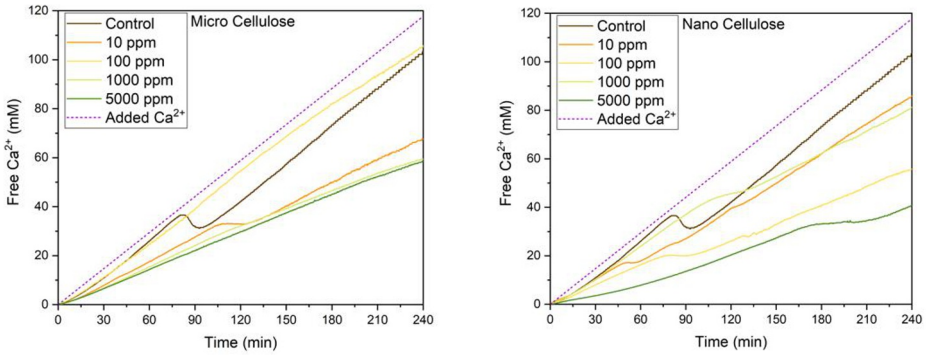

Fig. 1. Representative evolution of the free Ca^{2+} ion evolution with time in the presence of varying amounts of (a) micro-cellulose and (b) nano-cellulose. The control sample in both cases is drawn in dark-brown and the purple dotted line corresponds to the evolution of the total added Ca^{2+} to the reactor. A sudden change in slope of free Ca^{2+} signal represents the nucleation event.

The characterization of the reaction products was performed immediately after they were synthetized, to prevent as much as possible their premature carbonation. Since it has been demonstrated that the addition of natural organic additives promotes the formation of plate-like particles [20,22], X-ray diffraction was performed to calculate their presence. The average abundance of plate-like particles of portlandite was measured using the intensity ratio between the 001 Bragg peak and the principal diffraction peak of portlandite (i.e., 101) [18]. The obtained values are reported in Table 1. In the case of micro-cellulose additives, this analysis was performed only on the sample at 10 ppm, since there were no diffraction signals detected for the other concentrations. The latter means that a crystalline mineral is not present; however, an amorphous material could have been formed. The sample obtained from micro-cellulose dosed at 10 ppm, showed a slight reduction in the relative amount of plate like particles. Furthermore, the SEM micrographs (Fig. **2**) did not reveal any considerable difference with respect to the control sample. Both the control sample and that prepared with 10 ppm of micro-cellulose presented small rhombohedral crystals (5-10 µm in size) evidencing the formation of calcite due to early carbonation associated with the unavoidable air exposure during sample preparation. Moreover, portlandite rod-like crystals were predominantly present over plate-like crystals in full agreement with the XRD results.

For the samples made with 100, 1000 and 5000 ppm micro-cellulose, the evidence obtained with SEM (Fig. **2**) highlighted that there is no crystalline structure present. This was also evident from the lack of Bragg peaks in the diffractograms. Interestingly, the preliminary EDX analysis of the sample made with 1000 ppm micro-cellulose (Fig. **3**) evidences a Ca rich material with no crystalline features (i.e., lack of crystal faces). The obtained results may suggest the presence of an amorphous mineral phase. However, at this stage it is not possible to discern between amorphous calcium hydroxide (ACH) or amorphous calcium carbonate (ACC). Nonetheless, the textural/structural features observed in the samples do not entirely resembles those of ACC [37–39]. Furthermore, the EDS analyses Fig. **3** showed Ca, C, and O, which could be attributed to $CaCO_3$, but the presence of carbon and oxygen could also be due to the underlying cellulose. Therefore, further analyses, like FTIR and TGA, are required to confirm the nature of this amorphous material.

The intensity of the 001 Bragg peak increases with nano-cellulose concentration. In the limiting case of 5000 ppm nano-cellulose, the 001 peak completely dominates over the main 101 Bragg peak of portlandite This feature is typical of the increment in the amount of plate-like particles, as it is highlighted in Table 1. As observed, all the samples formed in the presence of nano-cellulose have a higher amount of plate-like particles than the control sample, except for that at 100 ppm.

The morphological analysis (Fig. **2**) of the crystals showed that at low concentrations of nano-cellulose (10 ppm), the sample resembles the control. However, in this case the rod-like portlandite crystals are smaller and co-exist with plate-like ones (circled in blue). Furthermore, a third structure was present, an aggregate made of many plate-shaped crystals (circled in red) that resembles a desert rose; this might be attributed to the potential presence of aragonite or vaterite [40,41]. At a nano-cellulose concentration of 100 ppm, portlandite crystals prevalently displayed a rod-like shape (i.e., elongated prisms). In this case it is possible to see a peculiar textural feature: a book-like opening in the (00.1) planes. This same rupture was also seen for 1000 ppm nano-cellulose, however for these latter samples the crystal separation is complete. This might help to explain the difference in plate-like abundance between these samples. The {00.1} faces of portlandite have a proclivity to break apart since these layers are held together by weak hydrogen bonds and Van del Waals forces [17]. It is possible that, if the nano-cellulose is partly attached to these faces, it will interrupt the proper bonding between these basal planes, weakening it and leading to the formation of two new surfaces. This is a positive aspect since an increment of the available surface area will also increase the reactivity of the mineral, which ultimately is the goal of cellulose addition. Finally, in the case of 5000 ppm concentration of nano-cellulose the largest amount of plate-like particles was calculated from XRD results. Two structures were observed in the SEM for this case (Fig. **2**), the typical portlandite hexagonal plate-like particles (circled in purple), and a complex structure of thin-layered spherulitic-shape minerals, similar to that often observed in aragonite or vaterite [40,41].

Table 1. Average plate-like particles abundance calculated from XRD results. The samples with 100, 1000, and 5000 ppm micro-cellulose are not reported since their diffractograms lack portlandite Bragg peaks.

Sample	Plate-like particle abundance [%]
Control	6.8
Micro-cellulose 10 ppm	5.8
Nano-cellulose 10 ppm	7.0
Nano-cellulose 100 ppm	5.6
Nano-cellulose 1000 ppm	8.1
Nano-cellulose 5000 ppm	26.9

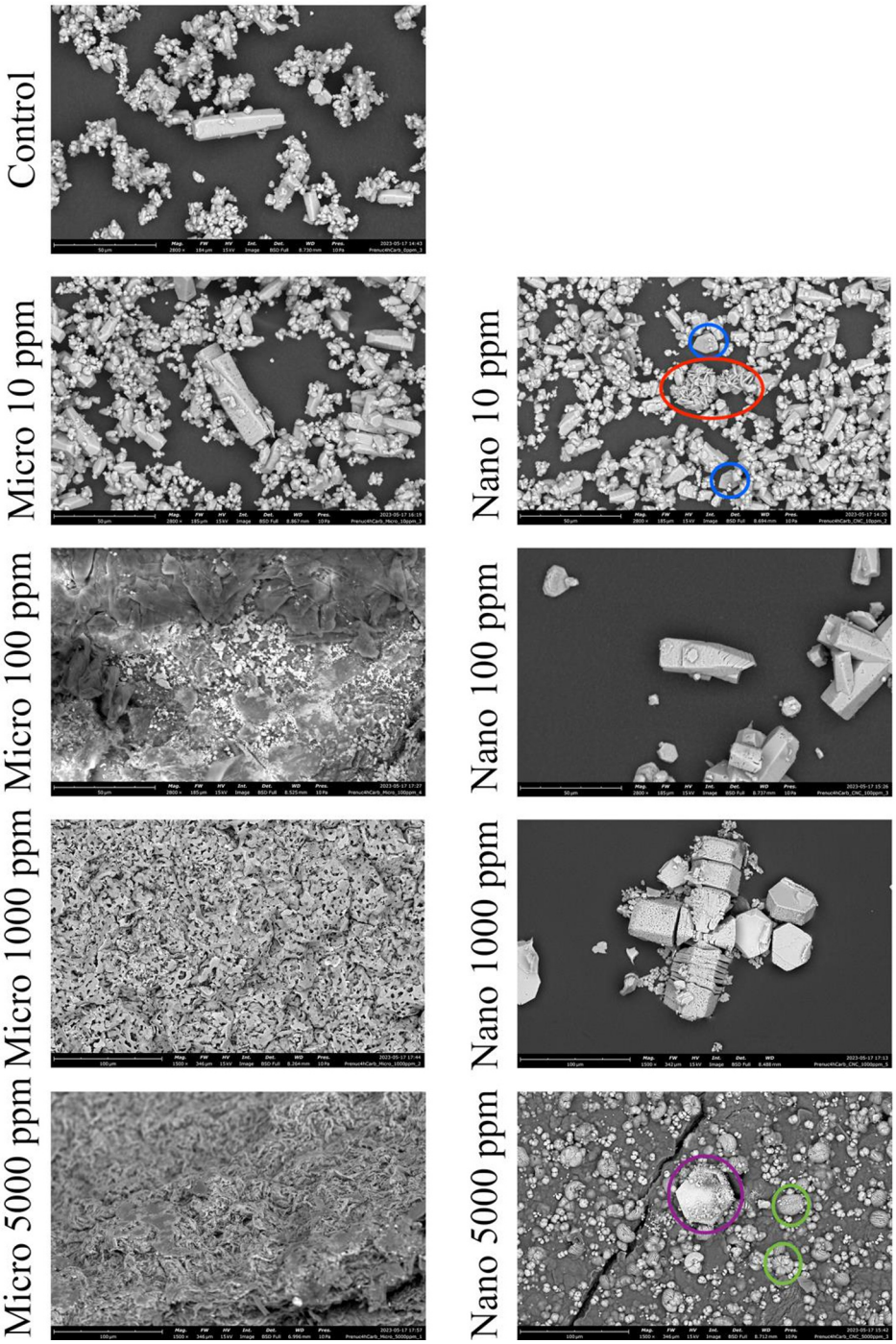

Fig. 2. Representative SEM micrographs of the resulting $Ca(OH)_2$ from titration experiments.

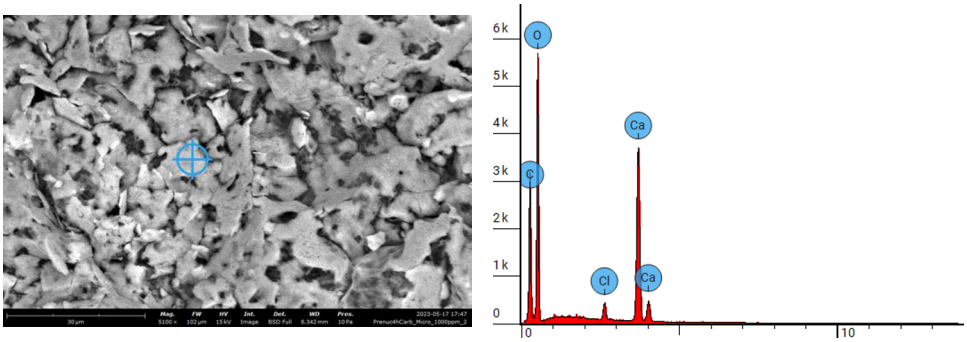

a b

Fig. 3: SEM image and EDX point analysis of the sample obtained with 1000 ppm of micro-cellulose.

3.2 Influence of cellulose on portlandite carbonation process

The process of carbonation was followed under atmospheric conditions for 20 days (Fig. **4**). The intensity ratio between the peaks of $CaCO_3$ at 1410 cm^{-1} and that of $Ca(OH)_2$ at 3635 cm^{-1} was calculated to analyse the progression of carbonation. Overall, higher intensity ratios were obtained for all the samples containing cellulose. At day 5, micro-cellulose addition promoted carbonation, speeding up the process. Then, the samples containing this additive follow an asymptotic behaviour as expected. The plateau is also observed for the nano-cellulose samples from day 12 onwards. Interestingly the promoting effect of adding nano-cellulose is slightly less marked than that of micro-cellulose. Meaning that possibly the amorphous material obtained in the presence of larger fibrils is more reactive than the plate-like particles.

The only particular case observed was that of nano-cellulose at 100 ppm. At day 12 the observed intensity of the carbonate band was larger than the general trend, followed by an apparent decrease in the carbonate content. The latter of course is not possible in this kind of materials, since $CaCO_3$ decarbonation under environmental conditions does not occur. Therefore, the obtained measurement of this sample in day 12 can be explained due to a local heterogeneity of carbonate content inside the sample. If this measurement was ignored, the general carbonation trend would be followed. In addition, this sample and the control are the only ones that do not reach a plateau, evidencing that the carbonation process was still ongoing.

The infrared measurements from day 0 and 20 and the diffractograms at day 20 for all samples are shown in Fig. **5**. At day 0, the presence of $Ca(OH)_2$ was identified by the peak at 3645 cm^{-1} indicative of the O-H stretching. The intensity of this peak decreased, as expected, during the carbonation process for all samples. However, after 20 days portlandite was still detected both on FTIR and XRD, evidencing that the carbonation was not fully completed. Moreover, at day 0, the characteristic sharp calcite peak (ν_2), at c.a. 875 cm^{-1}, was almost undetectable and is present only as a small shoulder of the 890 cm^{-1} peak. The latter does not correspond to the characteristic peaks of calcite or of portlandite crystals [42], however they could be associated with amorphous calcium carbonate (ACC), monohydrocalcite or a precursor in the process of carbonation [43,44]. Also at day 0, a peak at 3570 cm^{-1} was found in all samples, this could be correlated with water molecule vibrations from ACC [45,46]. This peak disappears for all the samples at 20 days.

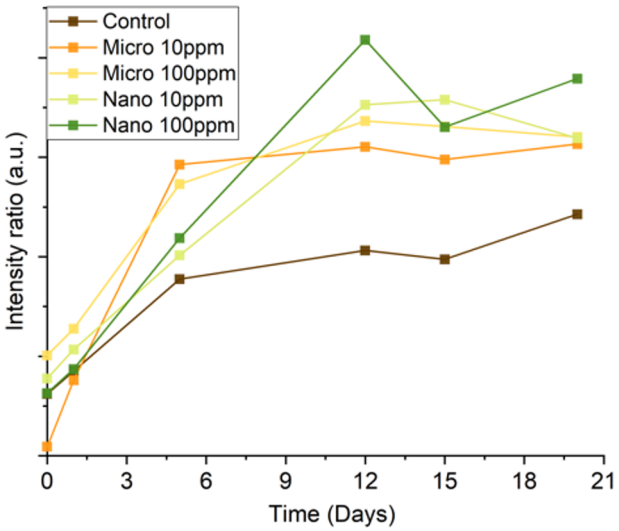

Fig. 4: Intensity ratio of FTIR peaks located at 1409 and 3635 cm^{-1} (calcite and portlandite respectively) vs. time for the control sample and samples containing 10 ppm, and 100 ppm of micro- and nano-cellulose.

Different calcium carbonate polymorphs can be recognized at day 20 of carbonation (**Fig. 5**). The control sample showed a characteristic peak of vaterite (745 cm^{-1}) [45], the presence of this polymorph was also confirmed by XRD. Also, this sample presented a broad and splitted peak in the region 1400 – 1550 cm^{-1}; this is a characteristic trade of amorphous calcium carbonate (ACC) or poorly crystalline $CaCO_3$ [45]; moreover, a small peak at 1080 cm^{-1} was observed, confirming the presence of ACC. The observed presence of ACC and vaterite, together with the minimal contribution of calcite (**Fig. 5**b) in this sample is evidence of its incomplete carbonation.

For those samples containing additives, in general the presence of calcium carbonates is associated with vaterite and/or calcite (identified by their distinctive bands at 745 cm^{-1} and 712 cm^{-1}, respectively); those peaks correspond to the O-C-O in-plane bending (ν_4) of the carbonate group [32,42,45]. The XRD of the sample with micro-cellulose dosed at 10 ppm confirms the presence of calcite together with vaterite. This is also evident from the distorted shape of the peak centred at 1430 cm^{-1} [47]. In contrast, the sample prepared in the presence of 100 ppm micro-cellulose is the only one showing calcite and not vaterite, both on FTIR and XRD. The presence of calcite in those samples prepared with micro-cellulose seems to be concentration dependent, which would agree with the carbonation kinetics results (**Fig. 4**). On the other hand, both samples made with nano-cellulose present calcite and vaterite (i.e., they show IR bands at 712 and 745 cm^{-1} respectively). Also, in both cases the 1400 – 1550 cm^{-1} region presents the broad split-shape found in ACC and/or poorly crystalline $CaCO_3$ [45,47]. However, the obtained maxima for this region are shifted with respect to those present in the reference samples, thus they could not be used as indicative. Moreover, the sample made with nano-cellulose also shows a small ACC band at 1080 cm^{-1}.

These results clearly indicate that the additives influence the formation of different calcium carbonate polymorphs during carbonation of portlandite crystals. Additionally, it is shown that micro-cellulose promotes a faster carbonation into calcite, which is the desired final mineral.

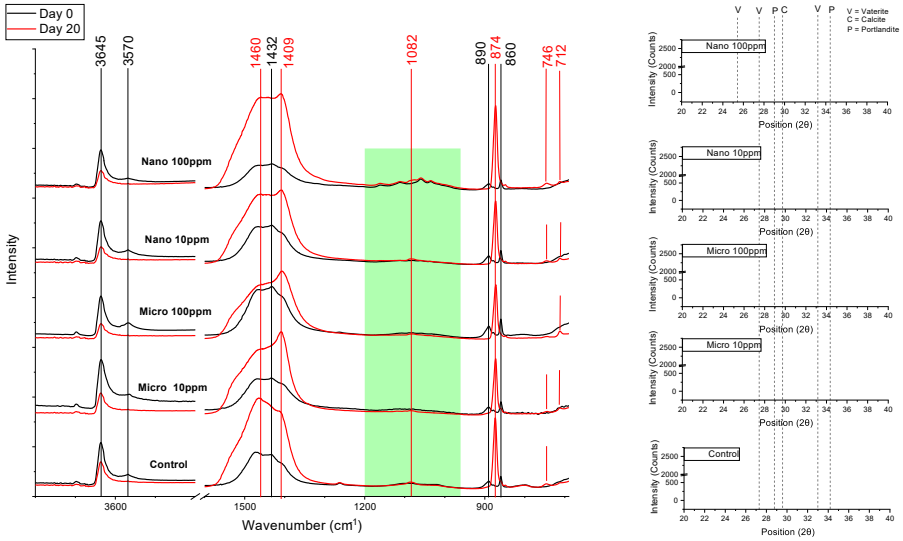

Fig. 5: a) Comparison of the FTIR spectra (from 1650 to 800 cm^{-1}) for the control sample and samples containing 10, and 100 ppm micro- and nano-cellulose at day 0 and 20. Wavenumbers from 3400 to 1600 cm^{-1} are ignored because do not contain any relevant information for this analysis. The region highlighted in green from 1200 – 950 cm^{-1} corresponds to the main peaks of cellulose. The diffractograms (b) were obtained at day 20 of carbonation. The principal phases observed are highlighted.

4 Conclusions

In the present work the role that micro- and nano-cellulose have on the precipitation and growth of $Ca(OH)_2$ crystals and their carbonation was studied.

The experimental results showed that the length of the cellulose fibres influences the effect that the additive has on the nucleation event and crystal growth process of $Ca(OH)_2$. Nano-cellulose acts as a nucleation accelerator when dosed in small quantities (10 ppm). Conversely, at higher concentrations (100 ppm or more), this material acts as a nucleation inhibitor. The inhibition is directly correlated to the quantity of dosed additive. Moreover, nano-cellulose addition generally promotes the formation of a larger population of plate-like crystals. The carbonation speed of portlandite samples with nano-cellulose was faster than the control, but at 100 ppm, full carbonation was not reached. Both calcite and vaterite polymorphs were present in these samples, along with ACC.

On the other hand, micro-cellulose resulted always in the delay of the nucleation, or even the apparent inhibition. However, the obtained products showed that for higher concentrations of additive, an amorphous material is obtained. This was evidenced by the lack of diffraction peaks and the calcium-rich material with no crystal shape observed with SEM-EDX. Further studies are required to determine exactly the nature of this amorphous phase. The carbonation process when micro-cellulose was used, proved to be the fastest and led to a predominant presence of calcite.

The obtained results indicate that the morphological modifications to $Ca(OH)_2$ induced by the additives have an impact on the reactivity of the resulting products. However, it is necessary to replicate these analyses on calcium hydroxide samples obtained through the hydration of CaO, to evaluate the real case scenario for lime-based mortars.

Acknowledgements: The present research was supported by the PhD Fellowship DOT1316197 (IMTR) CUP D45F21003710001 (Green) financed by Italian PON "Ricerca e Innovazione" 2014–2020 funding program. This research was partly supported by PON Ricerca e Innovazione 2014-2020 Risorse React Eu - DM 1062/2021 Azione IV.4, "Dottorati e contratti di ricerca su tematiche dell'innovazione" and Azione IV.6, "Contratti di ricerca su tematiche green". We also acknowledge funding from the European Union's Horizon 2020 research and innovation programme under Marie Sklodowska-Curie project SUBLime [Grant Agreement n°955986]: the Spanish Government grant PID2021.125305NB.I00 funded by MCIN/ AEI /10.13039/501100011033 and by ERDF A way of making Europe; Junta de Andalucía research group RNM-179; and University of Granada, Unidad Científica de Excelencia UCE-PP2016-05. Also, the authors would like to acknowledge Nicolò Massironi and Elena Vismara for their cooperation with the nanocellulose synthesis.

References

1. Isebaert, A.; Van Parys, L.; Cnudde, V. Composition and Compatibility Requirements of Mineral Repair Mortars for Stone – A Review. *Constr Build Mater* **2014**, *59*, 39–50, doi:10.1016/J.CONBUILDMAT.2014.02.020.
2. Santos, A.R.; do Rosário Veiga, M.; Matias, L.; Silva, A.S.; de Brito, J. Durability and Compatibility of Lime-Based Mortars: The Effect of Aggregates. *Infrastructures 2018, Vol. 3, Page 34* **2018**, *3*, 34, doi:10.3390/INFRASTRUCTURES3030034.
3. Kayan, B.A.; Jitilon, D.S.K.; Azaman, M.N.M. Low Carbon of Lime Plaster Repair: Life Cycle Assessment Approach in Achieving Sustainable Maintenance Management for Heritage Buildings. *Journal of Cultural Heritage Management and Sustainable Development* **2021**, *11*, 596–613, doi:10.1108/JCHMSD-05-2020-0068/FULL/PDF.
4. Zabalza Bribián, I.; Valero Capilla, A.; Aranda Usón, A. Life Cycle Assessment of Building Materials: Comparative Analysis of Energy and Environmental Impacts and Evaluation of the Eco-Efficiency Improvement Potential. *Build Environ* **2011**, *46*, 1133–1140, doi:10.1016/J.BUILDENV.2010.12.002.
5. United Nations Environment Programme *2022 Global Status Report for Buildings and Construction: Towards a Zero-emission, Efficient and Resilient Buildings and Construction Sector*; Nairobi, 2022;
6. Kylili, A.; Fokaides, P.A.; Jimenez, P.A.L. Key Performance Indicators (KPIs) Approach in Buildings Renovation for the Sustainability of the Built Environment: A Review. *Renewable and Sustainable Energy Reviews* **2016**, *56*, 906–915.
7. Yung, E.H.K.; Chan, E.H.W. Implementation Challenges to the Adaptive Reuse of Heritage Buildings: Towards the Goals of Sustainable, Low Carbon Cities. *Habitat Internationa* **2012**, *36*, 352–361.
8. Redden, R.; Crawford, R.H. Valuing the Environmental Performance of Historic Buildings. *Australasian Journal of Environmental Management* **2020**, 1–13.
9. Munarim, U.; Ghisi, E. Environmental Feasibility of Heritage Buildings Rehabilitation. *Renewable and Sustainable Energy Reviews* **2016**, *58*, 235–249.
10. Henry, A.; Stewart, J.; Heritage, E. *Practical Building Conservation: Mortars, Renders and Plasters*; 2011; ISBN 0754645592.
11. Dheilly, R.M.; Tudo, J.; Sebaïbi, Y.; Quéneudec, M. Influence of Storage Conditions on the Carbonation of Powdered Ca (OH) 2. *Constr Build Mater* **2002**, *16*, 155–161.
12. López-Arce, P.; Gómez-Villalba, L.S.; Martínez-Ramírez, S.; De Buergo, M.Á.; Fort, R. Influence of Relative Humidity on the Carbonation of Calcium Hydroxide

Nanoparticles and the Formation of Calcium Carbonate Polymorphs. *Powder Technol* **2011**, *205*, 263–269.
13. Van Balen, K.; Van Gemert, D. Modelling Lime Mortar Carbonation. *Mater Struct* **1994**, *27*, 393–398, doi:10.1007/BF02473442.
14. Groot, C. Repair Mortars for Historic Masonry: Effects of the Binder Choice on Durability. *Heron* **2016**, *61*, 33–56.
15. O'Brien, P.F.; Bell, E.; Santamaria, S.P.; Boyland, P.; Cooper, T.P. Role of Mortars in the Decay of Granite. *Science of the total environment* **1995**, *167*, 103–110.
16. Maravelaki, P.-N.; Kapetanaki, K.; Papayianni, I.; Ioannou, I.; Faria, P.; Alvarez, J.; Stefanidou, M.; Nunes, C.; Theodoridou, M.; Ferrara, L. RILEM TC 277-LHS Report: Additives and Admixtures for Modern Lime-Based Mortars. *Mater Struct* **2023**, *56*, 106.
17. Margalha, M.G.; Silva, A.S.; do Rosário Veiga, M.; De Brito, J.; Ball, R.J.; Allen, G.C. Microstructural Changes of Lime Putty during Aging. *Journal of Materials in Civil Engineering* **2013**, *25*, 1524–1532.
18. Rodriguez-Navarro, C.; Hansen, E.; Ginell, W.S. Calcium Hydroxide Crystal Evolution upon Aging of Lime Putty. *Journal of the American Ceramic Society* **1998**, *81*, 3032–3034.
19. Cazalla, O.; Rodriguez-Navarro, C.; Sebastian, E.; Cultrone, G.; De la Torre, M.J. Aging of Lime Putty: Effects on Traditional Lime Mortar Carbonation. *Journal of the American Ceramic Society* **2000**, *83*, 1070–1076.
20. Rodriguez-Navarro, C.; Ruiz-Agudo, E.; Burgos-Cara, A.; Elert, K.; Hansen, E.F. Crystallization and Colloidal Stabilization of Ca(OH)2 in the Presence of Nopal Juice (Opuntia Ficus Indica): Implications in Architectural Heritage Conservation. *Langmuir* **2017**, *33*, 10936–10950, doi:10.1021/ACS.LANGMUIR.7B02423/SUPPL_FILE/LA7B02423_SI_001.PDF.
21. Kang, S.H.; Kwon, Y.H.; Moon, J. Controlling the Hydration and Carbonation in Lime-Based Materials: Advantage of Slow Carbonation in CO2 Curable Construction Materials. *Constr Build Mater* **2020**, *249*, 118749, doi:10.1016/J.CONBUILDMAT.2020.118749.
22. Pesce, C.; Pesce, G.L.; Molinari, M.; Richardson, A. Effects of Organic Additives on Calcium Hydroxide Crystallisation during Lime Slaking. *Cem Concr Res* **2021**, *139*, 106254.
23. Gebauer, D.; Cölfen, H. Prenucleation Clusters and Non-Classical Nucleation. *Nano Today* **2011**, *6*, 564–584, doi:10.1016/J.NANTOD.2011.10.005.
24. Fu, H.; Gao, X.; Zhang, X.; Ling, L. Recent Advances in Nonclassical Crystallization: Fundamentals, Applications, and Challenges. *Cryst Growth Des* **2021**, *22*, 1476–1499.
25. Gebauer, D.; Cölfen, H.; Verch, A.; Antonietti, M. The Multiple Roles of Additives in CaCO3 Crystallization: A Quantitative Case Study. *Advanced Materials* **2009**, *21*, 435–439, doi:10.1002/ADMA.200801614.
26. Verch, A.; Gebauer, D.; Antonietti, M.; Cölfen, H. How to Control the Scaling of CaCO3: A "Fingerprinting Technique" to Classify Additives. *Physical Chemistry Chemical Physics* **2011**, *13*, 16811–16820, doi:10.1039/C1CP21328H.
27. Rodriguez-Navarro, C.; Burgos-Cara, A.; Di Lorenzo, F.; Ruiz-Agudo, E.; Elert, K. Nonclassical Crystallization of Calcium Hydroxide via Amorphous Precursors and the Role of Additives. *Cryst Growth Des* **2020**, *20*, 4418–4432, doi:10.1021/ACS.CGD.0C00241/ASSET/IMAGES/LARGE/CG0C00241_0007.JPEG.

28. RAO, A.; Berg, J.K.; Kellermeier, M.; Gebauer, D. Sweet on Biomineralization: Effects of Carbohydrates on the Early Stages of Calcium Carbonate Crystallization. *European Journal of Mineralogy* **2014**, *26*, 537–552, doi:10.1127/0935-1221/2014/0026-2379.
29. Rosato, L.; Stefanidou, M.; Milazzo, G.; Fernandez, F.; Livreri, P.; Muratore, N.; Terranova, L.M. Study and Evaluation of Nano-Structured Cellulose Fibers as Additive for Restoration of Historical Mortars and Plasters. *Mater Today Proc* **2017**, *4*, 6954–6965, doi:10.1016/J.MATPR.2017.07.025.
30. Xu, Q.; Xu, F.; Sun, C.; Huang, X.; Luo, H. Cellulose Nanocrystals Lime Mortar Based on Biomimetic Mineralization. *Constr Build Mater* **2023**, *366*, 130209, doi:https://doi.org/10.1016/j.conbuildmat.2022.130209.
31. D'Erme, C.; Caseri, W.R.; Santarelli, M.L. Effect of Fibrillated Cellulose on Lime Pastes and Mortars. *Materials 2022, Vol. 15, Page 459* **2022**, *15*, 459, doi:10.3390/MA15020459.
32. Lu, Q.; Cai, Z.; Wang, S.; Lin, F.; Lu, B.; Chen, Y.; Huang, B. Controlled Construction of Nanostructured Organic–Inorganic Hybrid Material Induced by Nanocellulose. *ACS Sustain Chem Eng* **2017**, *5*, 8456–8463, doi:10.1021/ACSSUSCHEMENG.7B02394.
33. Mohamadzadeh-Saghavaz, K.; Resalati, H.; Ghasemian, A. Cellulose-Precipitated Calcium Carbonate Composites and Their Effect on Paper Properties. *Chemical Papers* **2014**, *68*, 774–781, doi:10.2478/s11696-013-0513-7.
34. Gebauer, D.; Oliynyk, V.; Salajkova, M.; Sort, J.; Zhou, Q.; Bergström, L.; Salazar-Alvarez, G. A Transparent Hybrid of Nanocrystalline Cellulose and Amorphous Calcium Carbonate Nanoparticles. *Nanoscale* **2011**, *3*, 3563–3566, doi:10.1039/C1NR10681C.
35. Vismara, E.; Bertolini, G.; Bongio, C.; Massironi, N.; Zarattini, M.; Nanni, D.; Cosentino, C.; Torri, G. Nanocellulose from Cotton Waste and Its Glycidyl Methacrylate Grafting and Allylation: Synthesis, Characterization and Adsorption Properties. *Nanomaterials 2021, Vol. 11, Page 476* **2021**, *11*, 476, doi:10.3390/NANO11020476.
36. Gebauer, D.; Volkel, A.; Colfen, H. Stable Prenucleation Calcium Carbonate Clusters. *Science (1979)* **2008**, *322*, 1819–1822.
37. Myszka, B.; Schüßler, M.; Hurle, K.; Demmert, B.; Detsch, R.; Boccaccini, A.R.; Wolf, S.E. Phase-Specific Bioactivity and Altered Ostwald Ripening Pathways of Calcium Carbonate Polymorphs in Simulated Body Fluid. *RSC Adv* **2019**, *9*, 18232–18244.
38. Gal, A.; Habraken, W.; Gur, D.; Fratzl, P.; Weiner, S.; Addadi, L. Calcite Crystal Growth by a Solid-state Transformation of Stabilized Amorphous Calcium Carbonate Nanospheres in a Hydrogel. *Angewandte Chemie International Edition* **2013**, *52*, 4867–4870.
39. Cartwright, J.H.E.; Checa, A.G.; Gale, J.D.; Gebauer, D.; Sainz-Díaz, C.I. Calcium Carbonate Polyamorphism and Its Role in Biomineralization: How Many Amorphous Calcium Carbonates Are There? *Angewandte Chemie International Edition* **2012**, *51*, 11960–11970, doi:10.1002/ANIE.201203125.
40. Willinger, M.-G.; Polleux, J.; Antonietti, M.; Cölfen, H.; Pinna, N.; Nassif, N. Structural Evolution of Aragonite Superstructures Obtained in the Presence of the Siderophore Deferoxamine. *CrystEngComm* **2015**, *17*, 3927–3935.
41. Xu, A.W.; Antonietti, M.; Cölfen, H.; Fang, Y.P. Uniform Hexagonal Plates of Vaterite CaCO3 Mesocrystals Formed by Biomimetic Mineralization. *Adv Funct Mater* **2006**, *16*, 903–908, doi:10.1002/ADFM.200500716.

42. Sow, P.Y. IR-Spectroscopic Investigations of the Kinetics of Calcium Carbonate Precipitation, Universität Konstanz: Konstanz, 2016.
43. Neumann, M.; Epple, M. Monohydrocalcite and Its Relationship to Hydrated Amorphous Calcium Carbonate in Biominerals 2007.
44. Mehta, N.; Gaëtan, J.; Giura, P.; Azaïs, T.; Benzerara, K. Detection of Biogenic Amorphous Calcium Carbonate (ACC) Formed by Bacteria Using FTIR Spectroscopy. *Spectrochim Acta A Mol Biomol Spectrosc* **2022**, *278*, 121262.
45. Andersen, F.A.; Brecevic, L.; Beuter, G.; Dell'Amico, D.B.; Calderazzo, F.; Bjerrum, N.J.; Underhill, A.E. Infrared Spectra of Amorphous and Crystalline Calcium Carbonate. *Acta Chem. Scand* **1991**, *45*, 1018–1024.
46. Politi, Y.; Arad, T.; Klein, E.; Weiner, S.; Addadi, L. Sea Urchin Spine Calcite Forms via a Transient Amorphous Calcium Carbonate Phase. *Science (1979)* **2004**, *306*, 1161–1164.
47. Zhang, Z.; Xie, Y.; Xu, X.; Pan, H.; Tang, R. Transformation of Amorphous Calcium Carbonate into Aragonite. *J Cryst Growth* **2012**, *343*, 62–67.